Key Engineering Materials
ISSN: 1662-9795, Vol. 926, pp 349-357
doi:10.4028/p-0rss1k

Submitted: 2021-11-30
Accepted: 2022-02-18
Online: 2022-07-22

3D Modeling of Polymer Selective Laser Sintering Process : Laser–Polymer Interaction Modeling

Lan Zhang[a*], M'hamed Boutaous[b], Shihe Xin[c]

Univ Lyon, CNRS, INSA-Lyon, Université Claude Bernard Lyon 1, CETHIL UMR5008, F-69621, Villeurbanne, France

[a]Lan.zhang@insa-lyon.fr, [b]mhamed.boutaous@insa-lyon.fr, [c]shihe.xin@insa-lyon.fr

Keywords: Selective laser Sintering, Scattering, Temperature Distribution

Abstract. During selective laser sintering (SLS) process, the laser transmission in the polymer powder bed and solid polymer is different. The laser interaction with the powder bed splits into absorption, reflection and scattering three parts. The photon scattering between the polymer particles leads laser repeated absorption by particles, changes the photon's traveling directions, and further influences the temperature distribution at the scanning laser area. New distribution and attenuation coefficients need to be introduced for correcting the results. For better simulating the photons travel ways, we introduce the modified Monte-Carlo method and Mie-Scattering theory to predict laser distribution in the polymer powder bed, by considering the scattering phenomenon. This paper analyses how the initial porosity influences the maximum temperature, laser attenuation rate and porosity change rate. The results show that lower porosity promoting the laser scattering phenomenon, decreasing the maximum temperature and the powder porosity change rate.

Introduction

Selective Laser Sintering (SLS) belongs to the additive manufacture, which is a powder bed fusion technique, used in polymer manufacturing industry. The heat energy comes from the laser source. The laser-powder bed interaction model is an important part for simulating the SLS process, which involve the properties of the powders, energy conversion and heat transfer. For better simulating the laser transmission, the laser scattering model was introduced. Liu et al. [1] used the Monte-Carlo method to model the laser distribution in the powder bed, and demonstrated that the scattering phenomenon modifies the laser distribution in the powder bed. Zhou et al.[2] formulated the Monte Carlo based ray tracing algorithm to simulate the laser photons transmission in the bimodal random packing structures composed of particles, and examined the influence of particle sizes and emissivity. Considering the scattering, the scattering coefficient, radius of the particle, porosity of the powder bed are the three important parameters influencing the laser scattering in the powder bed. The scattering coefficient influences the laser travel direction, affected by laser types and the material's properties. We choosed CO_2 laser (10.5 μm wavelength) as heat source and PA6 material as an example to study the additive manufacturing process. The laser reflection is around 4%, and the scattering coefficient is 0.93 for PA6 with CO_2 laser.[3]. The photon travel distance indicates the photons' attenuation efficiency. It is influenced by the radius of particles and porosity of the powder bed. The common initial porosity of the PA powder bed is in the range of 0.4 - 0.6, and the diameter of PA powders are in the range of 10 μm to 100μm [4, 5]. In our simulation, the powder bed is considered as a continual homogeneous medium. The energy equation is formulated for the homogeneous medium and the finite volume methods (FVM) are established to solve it. Major involved multi-physical transient phenomena are melting, coalescence, densification and crystallization, and are taken into account by appropriate models based on the previous work [6].

This work aims at analysing the influence of the powder bed density on temperature distribution and the final sample density and making a comparison between numerical and experimental results. The paper is organized as follows: First, the multiphysical models and the material characteristics are presented, then the validation of the models with comparison to results from the IR camera, finally some simulation obtained results are presented and commented.

Mathematical Models

The heat transfer equation during SLS process in transient conditions is the following:

$$\rho C_p \frac{\partial T}{\partial t} = \nabla(\lambda \nabla) + Q + S_f + S_c \tag{1}$$

where T is the temperature of the homogeneous medium, ρ, C_p, and λ are respectively the equivalent density, specific and thermal conductivity of the homogenized powder bed, Q is the heat source from the laser beam, S_f is the melting latent heat absorbed by the polymer, and S_c is the crystallization enthalpy during the cooling step.

The density(ρ), the specific heat (C_p) and the thermal conductivity(λ) of the homogenized powder bed are calculated using the mixing law and Maxwell model:

$$\rho = (1-\varphi)\rho_p + +\varphi\rho_g \tag{2}$$

$$C_p = [(1-\varphi)(\rho_p(C_p)_p + \varphi\rho_g(C_p)_g]/\rho \tag{3}$$

$$\lambda = \lambda_g \frac{1+\gamma(d-1)(1-\varphi)}{1-\gamma(1-\varphi)} \tag{4}$$

$$\gamma = \frac{\lambda_p - \lambda_g}{\lambda_p + (d-1)\lambda_g} \tag{5}$$

where φ is the porosity, d is the geometric factor, and 'p' and 'g' indicate the polymer phase and the gas phase.

As the boundary conditions, convective and radiative heat losses are considered on the powder bed top surface:

$$-k\frac{\partial T}{\partial n} = -h_{tot}(T - T_{ext}) \tag{6}$$

$$h_{tot} = h + \varepsilon\sigma(T^2 + T_{ext}^2)(T + T_{ext}) \tag{7}$$

where h equal to 15 $\mathrm{W}m^{-2}K^{-2}$ is natural convection coefficient, ε equal to 0.8 is the surface emissivity, σ is the Stefan-Boltzman constant, T_{ext} is the ambient temperature(469K) and n is the normal direction. At the bottom surface, adiabatic condition is applied:

$$-k\frac{\partial T}{\partial n} = 0 \tag{8}$$

Modeling the laser transmission in the powder bed is the first important part in a SLS numerical model. The volume heat source usually is calculated by the Beer-Lambert methods in the traditional methods[7]. To consider scattering, we choose to introduce the modified Monte-Carlo methods and Mie theory to simulate the heat source transmission in the powder bed. It represents the laser beam by millions of photons, and model the photons random travel trace in the powder bed by the Mie theory. The scattering causes more energy distribution at the top surface of the powder bed, enlarges the laser effected zone and reduces the transmission depth, the detailed description of the Monte-Carlo method are shown in paper[1].

The heat flux provided by the laser beam can be written in a similar way as in the Beer-Lambert method as:

$$Q_{laser} = \frac{nP}{\pi b^2} e^{-\frac{(r-a)^2}{b}} e^{-\beta z} \tag{9}$$

where β is the average attenuation coefficient with depth, z represents the depth , a and b are the coefficients of the laser distribution at the radius direction, and n is the corrected scattering coefficient, which depends on powder density, powder radius, and laser reflection rate. The laser photons distribution in the powder bed, obtained after considering the scattering phenomenon, was used to fit the parameters of a, b and β.

The melting latent heat S_f is calculated by Voller's theory [8, 9]:

$$S_f = -(1-\varphi)\delta h \frac{\partial f_l}{\partial t} \tag{10}$$

where φ is the porosity of powder bed, δh, the total enthalpy latent absorbed by the polymer, is calculated by Laoadi's expression[10]:

$$\delta h = \rho_{pl} L + \rho_{pl} \int_{T_l}^{T} (C_p)_{pl} d\theta - \rho_{ps} \int_{T_s}^{T} (C_p)_{ps} d\theta \tag{11}$$

$$f_l + f_s = 1 \tag{12}$$

$$f_l(T) = (T - T_s)/(T_l - T_S) \tag{13}$$

In the above equations, L is the melting latent heat, f_l is liquid volume fraction varying along with temperature from 0 to 1 (f_l = 1 if $T > T_l$, and f_l = 0 for $T < T_S$) and f_s is solid volume fraction, f_l and f_s will be used to calculate ρ_p and C_P in Eq. 2 and Eq. 3 in the similar way.

Sintering is a process of compacting and forming a solid mass by heat or pressure without total melting of the materials. The sintering bonds are formed at the edge of spherical particles, making them to form a bigger body. The sintering consists of three steps: The first stage of sintering is the contact forming between the particles due to heating and the growing of the necks between grains. This process usually finished during the heating period, before the temperature cools down below melting temperature, and the interfacial energy reduces more than 50% as the neck grows. At this period, other parameters like pressure, density, particle size distribution and area of the free surface are important to determine the material's state. At the second stage, the particles form stable periphery grain boundaries, the smaller grains are eliminated and connected to the large grains. Large pores are formed at this stage and the densification changes with the grains enlargement and fusion. At the third stages, the porosity falls below 10%, materials continue transporting for filling the pores. The third stage is really slow compared to the previous two stages. The classic sintering models were established for amorphous materials using Frenkel model at the first stage, Mackenzie-Schuttleworth model at the third stage, and a combination of the two models for the second stage. The Frenkel model [11] used to describe the initial time for sintering is based on the balance of surface tension and the viscous dissipation:

$$\varphi(t) = 1 - \frac{1-\varphi_0}{[1-(\frac{\sin\theta(t)}{2})^2]^3} \tag{14}$$

The Mackenzie-Schuttleworth model [12] describes the final stage of densities above 0.9. This sintering model is based on closed pores and the shrinkage of spherical bubbles in a viscous matrix:

$$\frac{d\varphi}{dt} = \frac{-3\Gamma}{2a_0\eta}\varphi \tag{15}$$

where t represent the the sintering time, is surface tension, η is zero-shear viscosity of the melt polymer, and a_0 is the initial pore radius.

Finite volume methods is used to discretize the above equation and the parameters and polymer thermo-physical properties used in this articles are shown in Table 1. The details can be found in [6].

Results

Fig. 1 shows the calculation area for multi-sweep and multi-layers situations. The initial powder is spread on the machine plate uniformly. We assume an initial powder bed thickness about $1200\mu m$, and the thickness of new added layers is equal to $100\mu m$. The preheating temperature usually close to the melting starting temperature, is set to 469K in our simulation. The new layers addition is done

Table 1: Parameters and properties used in model.

Parameter and Property	Value
Diameter of the laser beam $[\mu m]$	450
Anisotropy factor, g	0.93
Laser power $[W]$	13
Scanning space $[\mu m]$	220
Speed of the laser $[m/s]$	3.5
Relative density	0.56,0.47,0.35
Average diameter of the grain $[\mu m]$	60
Attenuation coefficient of solid PA6	17000
Preheating temperature of the powder $[K]$	469
Initial melting temperature $[K]$	471
Finish melting temperature $[K]$	489
Thickness of each layer $[\mu m]$	100
Thickness of initial layer $[\mu m]$	1200
Number of the layers	10

always after the previous heating parts cold down to the preheating temperature. The laser moving directions are shown in the picture. The laser moving speed, input laser energy and space between two sweeps are the principal parameters controlling the laser power transmission in the powder bed.

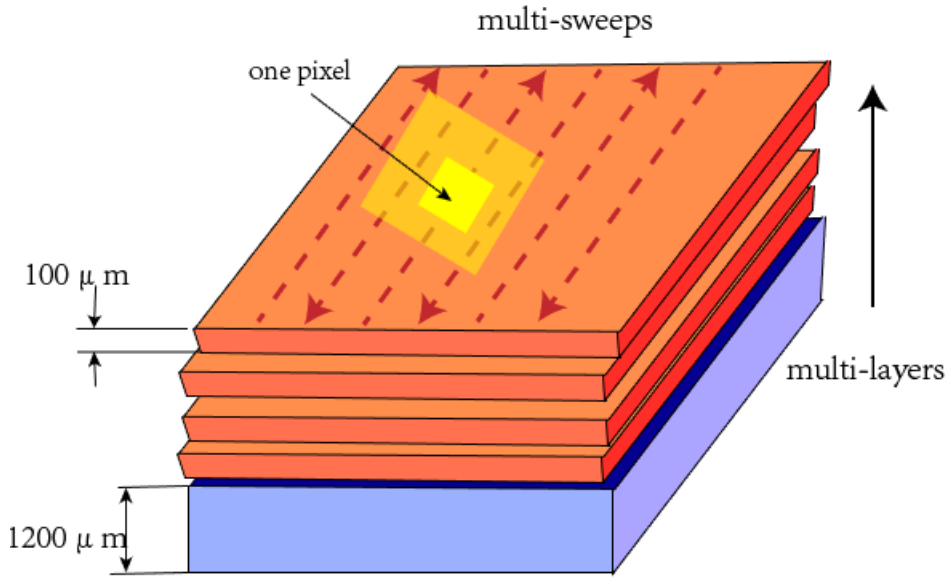

Fig. 1: Schematic view of the model with three scanning tracks in the powder layer.

The photons propagation traces in the powder bed, simulated using modified Monte Carlo method, are shown in Fig. 2. In Monte-Carlo methods, we assume the laser only absorbed by the polymer particles, and the laser absorption rate follows the Beer-Lambert attenuation method. The random scattered photons enlarge the photons radiative area at the surface and decrease the laser distribution in the depth direction. The update distribution coefficient a, b and β of laser energy Eq. (9) are all from this photons' scattering map, where a equals around $1.28e-4$ and b equals around $3.168e-4$, which is hardly influenced by the powder bed density.

The attenuation coefficients β variation with five powder beds initial densities are shown in Fig. 3. The common PA6 powder bed density for SLS process is 0.47. However, the irregular powder shape and the uneven distribution of particle size change the powder density. The irregular particles

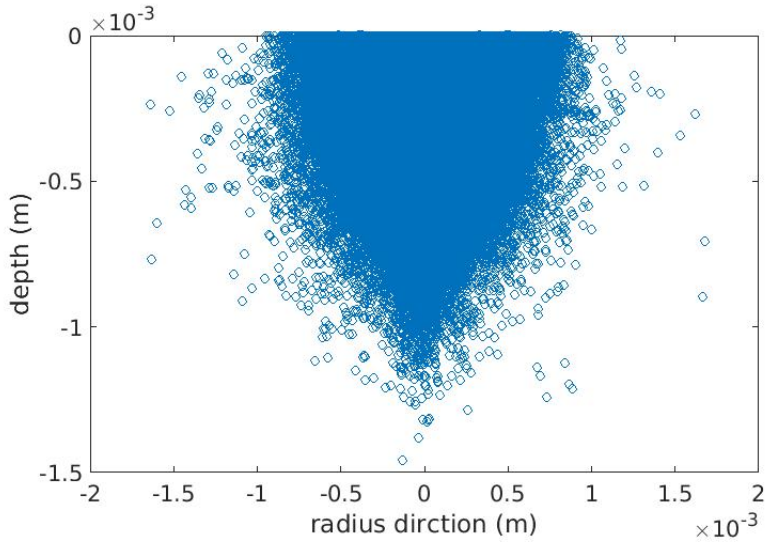

Fig. 2: Distribution of photons positions, MC methods.

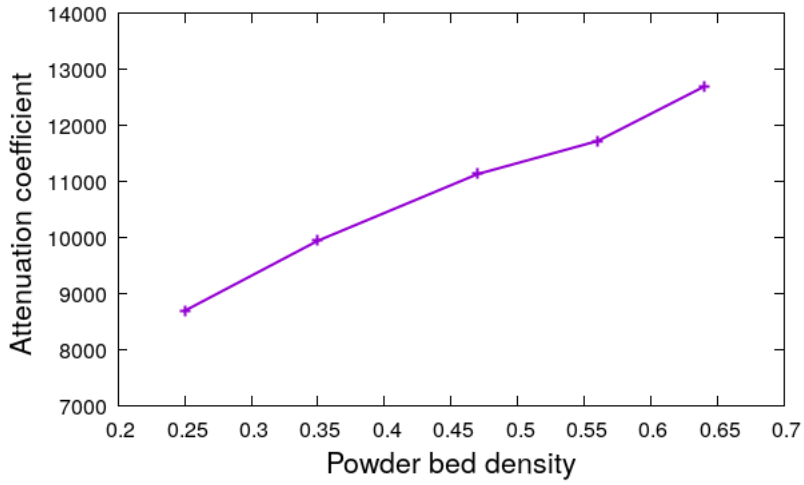

Fig. 3: Attenuation coefficient change with powder beds' density.

shape loosens particles arrangement, and result in a lower density. The irregular particles diameter distribution lead to higher density, because the smaller particles may take the clearance space between the particles. The laser attenuation coefficients increase with the powder bed density increase, because higher density not only increases the absorption, also improves the chance of photons scattering, which cause the photons repeated absorption by one polymer particle. Fig. 3 also illustrates that high density promotes the scattering phenomena and enlarges the heating influence area at radius direction.

The compared temperature profiles, calculated numerically and measured using IR camera, are shown in Fig. 4. Using IR camera to observe surface temperature was helpful, as it is difficult to insert any temperature probes under laser radiation. But it needs a powerful and rapid camera as the process involves very quick phenomena to be measured. In fact, during the SLS process, the sample temperature reachs a high level at a short period, usually smaller than 0.001s, then cools down to the preheating temperature within 0.3 s. The IR camera shutter time is around 0.0056 s, it is hard to catch the maximum temperature but enough to reflect the temperature variation with time. The scanning length and direction change delay time, which influence the comparison result. The travel length influences the maximum temperature because longer scanning length decrease the overlap effect which due to prolong the previous laser scanning . The laser has short delay time when changes the moving direction.

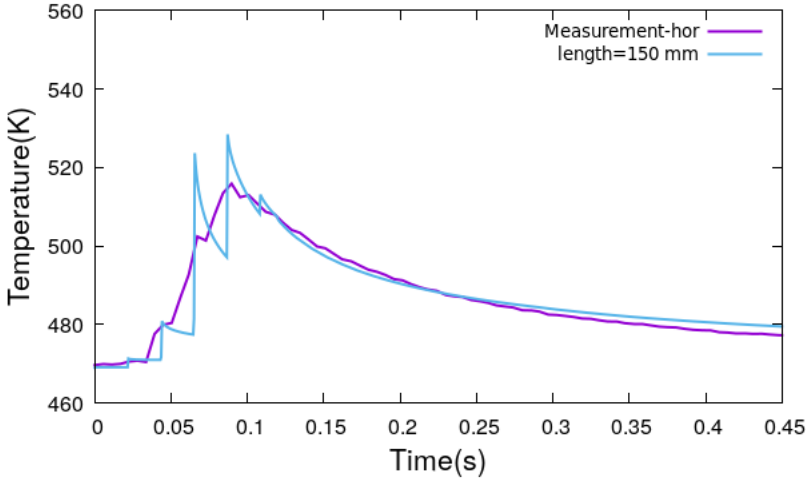

Fig. 4: Comparision of simulation and experimental thermal profile(power=13w).

The sample length is 0.05 m, but the delay time is hard to measure, therefore, we prolong laser travel scanning length for substitution the staying time. We chose the middle of sample for comparing the temperature, and the delay time equal 0.08m laser moving time in this part.

A successful maximum temperature and cold rate comparison result is show in Fig. 4, the simulation maximum temperature is 531K, which is well compared with the measured surface temperature (around 518K). Note that the thermal kinetics are well comparable between the modeled results and the measurement.

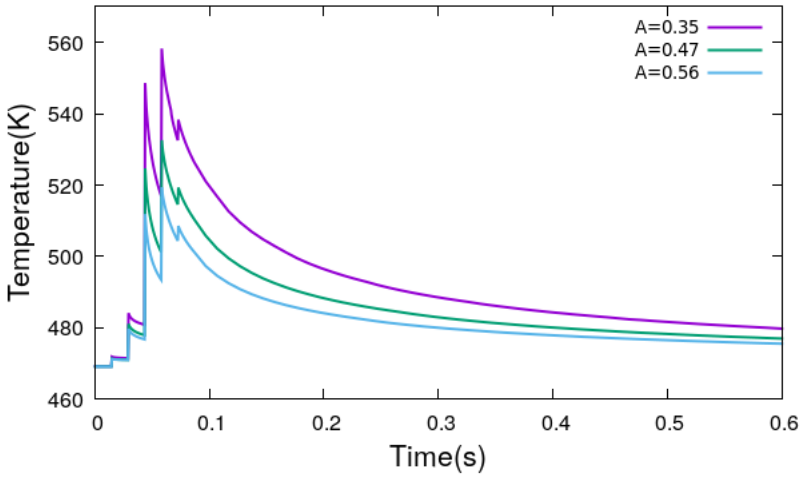

Fig. 5: Porosity-Temperature with different powder density.

Fig. 5 presents the temperature-time profile with various powder bed initial density. The highest maximum temperature is around 560K at powder density of 0.35, which is roughly 40K higher than the maximum temperature with powder density of 0.56. The heat influence time is smaller than 1s, however, in practice, the waiting time for adding new powders is longer than 5s, it means that the surface temperature monitor is independent for each layers. In this part, because the temperature-time profiles are similar for each layers, we decide to choose one layer to be studied for representing all layers. The particles arrangement formation and the morphology of the powders influence the particles alignment, thereby further affect the laser photons distribution in the powder bed. Higher powder bed density lead more energy absorption by the topper layers with the same input power. However, the maximum temperature is lower with the high density powder bed compared to lower density. These is

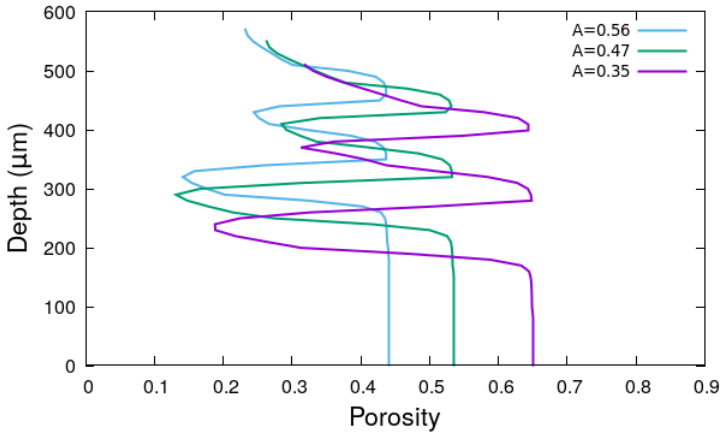

Fig. 6: Porosity predict in z-coordinates with different powder density.

due to the melting latent heat. So the maximum temperature is not just decided by the absorbed laser energy, but also influenced by the melting process which concerns more mass to be melted in the same volume. Knowing that, with polymers materials, the phase change happens with a slow temperature increase, this leads to lesser maximum temperature that in case of less density. The melting process absorb energy to promote molecular breakage, which display surface sink shape. Furthermore, the tight alignment powder bed causes more particles concentration by one unite simulated area, that lead more energy absorbed by the materials for melting, instead for increasing the surface temperature.

The porosity prediction along vertical coordinate is shown in Fig.6. In this figure, we presented the porosity evolution for three layers, after simulating a sample with ten layers. The porosity changing ranges are between 0.42 and 0.23 for the case of 0.56 initial density, between 0.53 and 0.27 in case of 0.47 initial density and between 0.65 and 0.32 in case of 0.35 initial density. The porosity change rate are 43%, 49% and 51% respectively. of course, these evolution of densities are obtained for a given energy density. The finale density of samples were decided by the initial powder bed density, it illustrates the importance of powders' shape and particles' diameter distribution, which influence the initial powder bed density. The Z shape of the density evolution within a layer of a powder bed is due to the interface density between two layers. When adding a new layer, as the new powder has lower temperature, particles need more time at high temperature to be welded to the old melted layer. As the process is very quick, and the molecules diffusion depends on the energy density supplied by the laser and also on the repetition times of each polymers molecules. This lead to less dense zones at the interfaces, and more dense others zones where the grains are completely melted. The dimensions of those alternating zones depend on the kinetics of heat diffusion and the time during which the particles stays at high temperature than their melting one. for the same reasons, a contrary conclusion was got when we study the porosity change rate. The porosity change rate in high powder density is smaller than in low density. It is because the higher maximum temperature and longer high temperature maintains time were got in low density powder bed (show in Fig. 5), which promoting the sintering process.

Fig. 7 shows the shrinkage thickness under three set of densities, the shrinkage thickness increases when the powder bed density decreases. The low density with loose iterative structure collapse easier than high density structure. Lower density situation gets higher maximum temperature and longer high temperature staying time that promote particle's necks forming and leave more time for inserted gas escaping from the molten part.

Conclusion

The scattering phenomenon was introduced in SLS laser-power model for better simulating the laser transformation traces in powder bed. Once the photons hit on the particles, the photon's travel di-

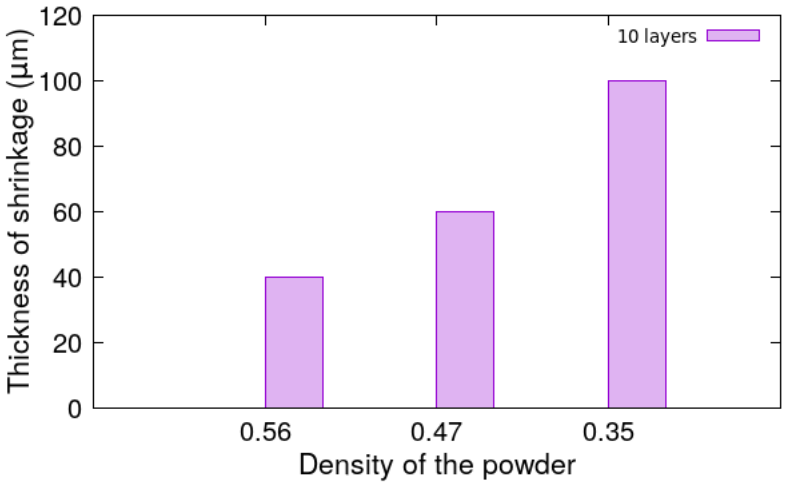

Fig. 7: Shrinkage rate with different density.

rection was changed and the direction were decided by Mie theory. The laser attenuates quickly in high density powder bed because tight stacking powders enhance the absorption phenomenon by increasing the laser traveling length through the materials, and high density also increase scattering phenomenon to lead laser photons repeatedly absorbed by the particles. So, the high density powder bed enhances the scattering and leads more energy distribution at the surface of the powders. Then, a successful comparison is preformed between the simulated temperature-time profile and experimental profile, obtained in a real industrial SLS machine based on IR camera, which proving the reliability of our model. Moreover, the simulation results of temperature time variation, porosity prediction along depth, shrinkage thickness for different porosity are presented. These show the high density powders are easier getting a tight, low porosity sample comparing to low density powders. However, a high sintering rate and a high temperature distribution were got in low density powder bed, because less energy was absorbed for melting the particles, but the low initial densities lead to more important shrinkage of the material which consequently can affect the dimensions of the sintered parts.

References

[1] Xin L, Boutaous M, Xin S, et al. Numerical modeling of the heating phase of the selective laser sintering process[J]. International Journal of Thermal Sciences, 2017, 120: 50-62.

[2] Zhou J, Zhang Y, Chen J K. Numerical simulation of laser irradiation to a randomly packed bimodal powder bed[J]. International Journal of Heat and Mass Transfer, 2009, 52(13-14): 3137-3146.

[3] Laumer T, Stichel T, Nagulin K, et al. Optical analysis of polymer powder materials for selective laser sintering[J]. Polymer Testing, 2016, 56: 207-213.

[4] Kačianauskas R, Maknickas A, Kačeniauskas A, et al. Parallel discrete element simulation of poly-dispersed granular material[J]. Advances in Engineering Software, 2010, 41(1): 52-63.

[5] Chen P, Wu H, Zhu W, et al. Investigation into the processability, recyclability and crystalline structure of selective laser sintered Polyamide 6 in comparison with Polyamide 12[J]. Polymer Testing, 2018, 69: 366-374.

[6] Mokrane A, Boutaous M, Xin S. Process of selective laser sintering of polymer powders: Modeling, simulation, and validation[J]. Comptes Rendus Mécanique, 2018, 346(11): 1087-1103.

[7] Peyre P, Rouchausse Y, Defauchy D, et al. Experimental and numerical analysis of the selective laser sintering (SLS) of PA12 and PEKK semi-crystalline polymers[J]. Journal of Materials Processing Technology, 2015, 225: 326-336.

[8] Voller V R, Swaminathan C R. ERAL Source-based method for solidification phase change[J]. Numerical Heat Transfer, Part B Fundamentals, 1991, 19(2): 175-189.

[9] Voller V R, Swaminathan C R. General Source-Based Method for Solidification Phase Change[J]. Numerical Heat Transfer (Part B): 175-189.

[10] Laouadi A, Lacroix M, Galanis N. A numerical method for the treatment of discontinuous thermal conductivity in phase change problems[J]. International Journal of Numerical Methods for Heat Fluid Flow, 1998.

[11] Wadsworth F B, Vasseur J, Llewellin E W, et al. Sintering of viscous droplets under surface tension[J]. Proceedings of the Royal Society A: Mathematical, Physical and Engineering Sciences, 2016, 472(2188): 20150780.

[12] German R M. Coarsening in sintering: grain shape distribution, grain size distribution, and grain growth kinetics in solid-pore systems[J]. Critical reviews in solid state and materials sciences, 2010, 35(4): 263-305.